Proceedings Paper:
Garufo, A, Sberna, P, Carluccio, G et al. (10 more authors) (2019) Pulsed Photoconductive Connected Slot Array Operating at the Sub-mm Wavelength Band. In: Proceedings of the 14th European Microwave Integrated Circuits Conference. 14th European Microwave Integrated Circuits Conference, 30 Sep - 01 Oct 2019, Paris, France. , pp. 266-269. ISBN 978-2-87487-056-9

10.23919/EuMIC.2019.8909489

Pulsed Photoconductive Connected Slot Array Operating at the Sub-mm Wavelength Band

A. Garufo[#1], P. Sberna[#1], G. Carluccio[#1], J. R. Freeman[#2], D. R. Bacon[#2], L. Li[#2], J. Bueno[#3], J. J. A. Baselmans[#3] , E. H. Linfield[#2], A. G. Davies[#2], I. E. Lager[#1], N. Llombart[#1], A. Neto[#1]

[#1]Delft University of Technology, Delft, The Netherlands

[#2]University of Leeds, Leeds, United Kingdom

[#3]Netherlands Institute for Space Research, Utrecht, The Netherlands

{a.garufo, p.m.sberna, g.carluccio, i.e.lager, n.llombartjuan, a.neto}@tudelft.nl

{j.freeman, d.bacon, l.h.li, e.h.linfield, g.davies}@leeds.ac.uk

{j.bueno, j.baselmans}@sron.nl

Abstract — A novel pulsed photoconductive THz source is presented that is able to radiate mW-level average powers, over a large bandwidth by exploiting both the optical and electrical properties of photoconductive sources and the ultrawideband properties of connected antenna arrays. An optical system composed of a micro-lenses array splits the laser beam into N x N spots that host the active excitation of the antenna arrays. An "ad hoc" network has been adopted to bias the array active spots in order to implement a connected antenna array configuration. The array feeds a silicon lens to increase the directivity of the radiated THz beam. A slot array prototype has been designed, fabricated, and measured. The proposed solutions achieve excellent power radiation levels by making use of an accurate electromagnetic design. This solution can offer enhancements to any active system relying on pulsed photoconductive antennas.

Keywords — Photoconductivity, THz photoconductive antenna, THz radiated power, THz source, THz technology, THz time-domain measurement, connected array, ultra-wideband array.

I. INTRODUCTION

The emergence of a large variety of applications, for THz technology in recent years has been driven by the availability of photoconductive antennas (PCAs) that have provided power up to THz frequencies at relatively low cost, thanks to several breakthroughs in photonics and semiconductor technology [1]–[2]. PCAs are a combination of THz antennas and semiconductor materials driven by optical laser sources, that exploit photoconductivity to radiate power over large bandwidths, reaching THz frequencies. Currently, the power radiated by these devices is limited by the high dispersivity and poor radiation efficiency of the existing PCA designs [3]. These bottlenecks render the integration time to detect the THz signal longer than really necessary and, as a consequence, these devices are limited to short-range applications (e.g. spectroscopy). The maximum power emitted by a single PCA is limited by: (i) the maximum value of biasing voltage applied to the material, which can lead to the failure of the substrate material if it exceeds the voltage breakdown; (ii) the maximum laser power, exceeding this leading to the thermal failure of the device. Moreover, even before failure, large amounts of laser power and/or a high bias voltage lead to the saturation of the photocurrent [4], limiting the available power of the device. In order to increase the available radiated THz power, various PCA array structures have been proposed in the recent years [5]–[6]. However, all these technological solutions are electromagnetically inefficient when operating over wide bandwidths in a pulsed system. This is because they all rely on array arrangements of electrically short radiating elements, which are intrinsically efficient over a narrow band, only.

In this work, we describe the design and the analysis of connected array of photoconductive sources (PCCA), a concept that was presented for the first time in [7]. A connected array (CA) of photoconductive sources can be viewed as a modification of a CA antenna, a structure with proven intrinsic wideband radiation performance. This property makes CA's of sources suitable to efficiently radiate the wideband pulses generated in the optically pumped photoconductive gaps. The design, presented in this paper targets at large submillimeter wavelength spectra, covering a bandwidth at -5dB from 0.1 THz to 0.6 THz, and radiating **mW-level** average power.

II. PCCA BASED SOURCE FOR SUB-MM WAVELENGTH

The PCCA architecture is shown in Fig. 1(a). The design involves two components: (i) the CA which includes the biasing network; (ii) the optical system used to excite the photoconductive gaps of the array cells, Figs. 1(b), 1(c). The optical system consists of an array of micro-lenses, which splits the laser beam and focuses a portion of the beam on each gap in the array. The CA structure has two functions: biasing the gaps and ensuring the wideband radiation at THz frequencies. For the biasing function, it uses a connected biasing network that feeds the gaps in series, providing the bias voltage at each array cell to accelerate the free carriers excited by the optical pulses absorbed in the semiconductor. At THz frequencies, the CA radiates the electromagnetic (EM) energy associated to these transient electric currents. The array is coupled to a dielectric silicon lens to increase the antenna directivity of the THz radiation.

The following subsections elaborate on the design and the manufacturing of the connected slot array of photoconductive sources that radiate in the submillimeter bandwidth (<1THz).

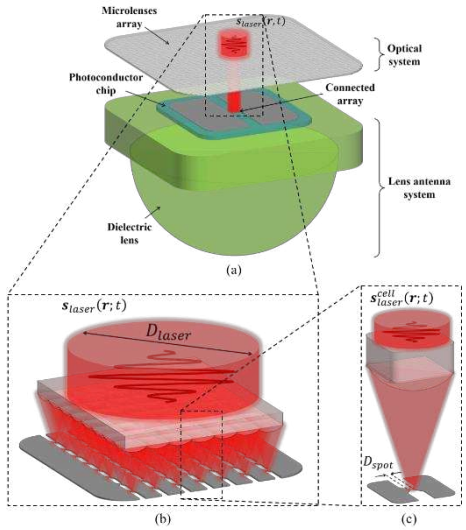

Fig. 1. The PCCA structure. a) General view of the system structure; b) the CA and its excitation optical network; c) detailed view of the cell excitation.

A. Array Design

The design of the arrays was carried out by taking into account the spectral energy distribution of the current pulse generated in the photoconductor. To this end, use was made of the linear equivalent model for pulsed photoconductive source, developed in [8], [9] for small bias voltages and laser excitations, where no saturation and screening effects are considered. As shown in [8], [9], for photoconductive sources most of the energy is contained in the lower frequencies part of the spectrum (< 1THz). The features of the employed laser are: maximum laser average power $P_{laser,max}$=0.5W, carrier frequency f_{laser} =375THz (central wavelength λ_{laser}=800 nm), pulse duration τ_p=100fs, and a repetition rate frequency f_p=80MHz. Due to the Gaussian power distributions typically produced by lasers, the available optical power P_{laser} will not be entirely focused on the gaps. Indeed, referring to Fig. 1, assuming a laser beam with diameter at -3dB equalling the array size, $D_{laser,ideal}=L_x=L_y$, and the micro-lenses focused laser spot at -3dB matching the gaps width $D_{spot,ideal}=W_x=W_y$, a 6dB total spillover loss has to be taken into account. For the optical system, a commercially available micro-lenses array has been adopted with a 100µm pitch, focal distance f=0.95mm, square rim, 100% fill-factor, and 96% of optical power transmission at wavelengths around 800nm. Resorting to the model in [8], an array of 5 x 5 cells has been considered, this size being deemed sufficient for mimicking the behaviour of an infinite array for the cells. The resulting overall dimensions of the array were 0.5mm x 0.5mm. The gap sizes of the cells of the arrays have been fixed to ideally match the -3 dB spot size of the laser sub-beams focused by the micro-lenses, i.e., $W_x=W_y=D_{spot}$ =7.5µm. All geometrical details of the array and its cells are listed in the caption of Fig. 2.

The array has been lithographically defined on a LT-GaAs semiconductor wafer. The details of the wafer can be found in [9]. Microscope pictures of the metallization, obtained by photolithography, are shown in the inset of Fig. 3. The design includes a silicon lens, with radius R_{lens}=5mm, and extension length $E_{lens}=0.18R_{lens}$, in order to get an overall extension length, including the thickness of the chip, equal to the ideal hyperhemispherical extension. A quarter-wavelength matching layer on the silicon lens at central frequency 0.4THz has been applied, in order to reduce the reflection at the lens-air interface. This matching layer consists of a 114µm high-purity parylene coating with relative permittivity ε_c=2.72.

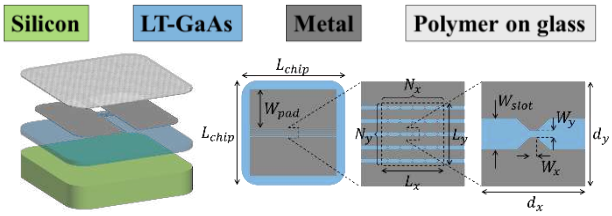

Fig. 2. The PCCA elements: blue slab = the photoconductive material chip; green thick slab = the silicon lens; dark-gray sheets = array metallizations; light-gray slab = the micro-lenses array. The array consists of $N_x=N_y=5$ square cells of dimensions $d_x=d_y=100$µm; array size $L_x=L_y=0.5$mm; bias pad width $W_{pad}=2.25$mm; overall chip dimension $L_{chip}=6$mm; slot width $W_{slot}=20$µm; gap size $W_x=W_y=7.5$µm.

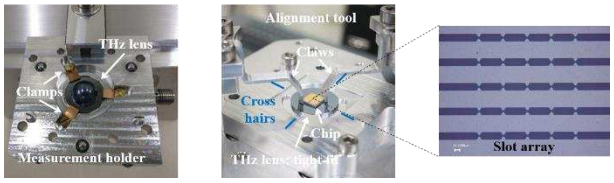

(a) (b) (c)

Fig. 3. Prototype of the PCCA: a) view of the THz lens (Top view): b) view of the chip, and PCB for biasing the array (Bottom view); c) picture at the microscope of the slot CA on the semiconductor chip.

B. Array Manufacturing

The device has been realized by assembling together, on top of each other, the micro-lenses array (MLA), the PCCA chip and the Si lens (see Fig. 3(a)-(b)). The distance between the MLA and the PCCA metallization plane is equal to the focal length of the micro lenses (950µm, with depth of focus ±40µm) for the efficient focalization of the laser radiation on the PCCA gaps. The MLA has been aligned with respect to the PCCA elements with an accuracy of 10µm. This margin offered the possibility to compensate for the alignment error by stirring the impinging laser beam. The PCCA chip is located at the centre (±10µm) of the Si lens. The devices, have been then attached on PCBs that are equipped with an SMA connector for the bias voltage application. The bias lines of the PCB are connected to the PCCA electrodes through wire bonding. The whole structure has been then mounted into an aluminium chassis of a 5 degree of freedom mounting stage. The mounting stage allows the micrometric alignment of the devices to the collimated laser beam and its stirring.

III. Estimated Performance and Measurements

The analysis of the arrays has been carried out following the procedure discussed in [9], using the equivalent theoretical model in [8] in conjunction with the EM analysis of the CA

and the Quasi-Optical (QO) channel of the measurement setup used for characterizing the prototype.

A. Array Radiation

The array geometry has been simulated weighting the excitation at each port, taking into account the illumination of the gaps provided by the optical system design discussed previously, and loading the ports with the impedances evaluated by using the equivalent circuit in [8]. The simulated active input impedances of the array cells, considering a laser power excitation of 500mW, are shown in Fig. 4. Both active resistances and reactances of the array cells oscillate around the values of the active resistance of the cell in an infinite CA configuration (red dash-dotted line in Fig. 4). This is due to the small number of array elements considered in this design. An increase in the active resistances manifests itself above 0.7THz as a result of the grating lobes onset. This is a direct consequence of the unit cell dimensions becoming comparable to the effective wavelength that, in turn, results in the out of phase coupling between the ports of adjacent unit cells.

By using the simulated radiation patterns of the arrays inside (Primary Field) and outside (Secondary Field) the dielectric lens, the gain of the array designs has been computed (see Fig. 5(a)). This takes into account the front-to-back losses, dielectric losses of the silicon, and the reflection losses at the lens interface including the effect of the matching layer. The gain does not include the matching efficiency between the active antenna and the source impedances.

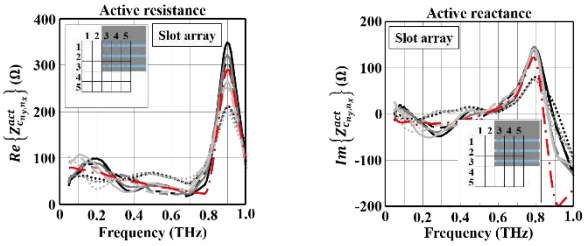

(a) (b)

Fig. 4. Active impedance of the slot array cells. Because of the symmetrical excitation of the array elements only the active impedances of the cells in a quarter of the arrays are shown. The red dash-dotted lines refer to the active resistances/reactances of the unit cell in an infinite CA configuration.

B. Quasi-Optical System

The measurement setup is composed of two 90° off-axis parabolic reflectors and a power meter coupled to the reflector by a conical horn antenna (WR-10). For the spectrum measurements the power meter has been replaced by an Electro-Optic (EO) crystal system for the detection of the THz pulses. To drive the laser and focus the laser beam on the PCCA, an optical sytem, ending with a telescopic lens system, was used. The laser beam diameter obtained by such telescopic lens system was D_{laser}=660μm. All the features of the reflectors system and the detector can be found in [9]. The measurement setup has been characterized in terms of efficiency of all stages across the radiated pulsed bandwidth. The entire QO channel used to couple the radiated energy to the detector can be characterized by the QO channel efficiency [9] η_{qo}, where the lens antenna efficiency η_l takes into account the front-to-back losses, the dielectric losses of the silicon, and the reflection losses at the lens interface, including the matching layer. The ohmic losses in the metallizations have not been considered since they are negligible. The reflectors system efficiency η_{rs} takes into account the spillover losses of the reflectors chain. The detector efficiency η_d considers the coupling losses between the reflectors system, the conical horn antenna, and the waveguide inside the detector. All these efficiencies are defined and discussed in detail in [9]. For the proposed array design the QO efficiency is shown in Fig. 5(b).

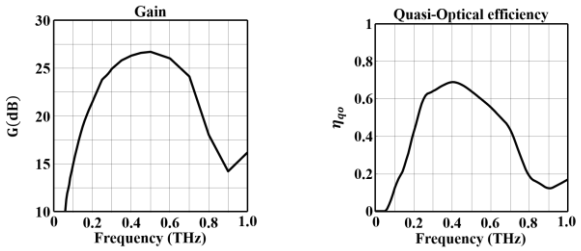

(a) (b)

Fig. 5. Simulated radiation performance: (a) gain of the array design, taking into account the front-to-back losses, the dielectric losses of the silicon, and the reflection losses at the lens interface including the effect of the matching layer; (b) efficiency of the QO channel, taking into account the lens efficiency η_l, the reflectors system efficiency η_{rs}, and the detector efficiency η_d.

C. Spectrum and Power Budget

The results of the EM analysis of the array and the measurement setup has been used, jointly with the equivalent circuit for pulsed photoconductive antennas presented in [8], [9], to compute the radiated and measured energy spectra and average power of the photoconductive array design: $E_m(\omega) = \eta_{qo}(\omega)\, E_s(\omega)$, where E_s is the spectral energy density generated by the array, η_{qo} is the QO efficiency, and E_m is the measured spectral energy density estimated by the model. Fig. 6 shows the generated and measured spectral energy density for an optical excitation of 500mW and a bias voltage of 200V.

Since the PCCA radiates periodically with a period $T_p = 1/f_p$, with f_p being the repetition rate of the laser excitation, the average power associated with each spectrum can be calculated by integrating the relevant energy spectral density, and dividing by the laser repetition rate T_p, as in [8]. Fig. 7(a) shows the comparison between the measured power of the prototype and the detected average power P_{meas} estimated by the model as a function of the applied voltage and for different laser excitations.

Table 1 shows the power budget of the PCCA prototype for 500mW laser power excitation and for different biasing voltages. The table shows that the available power $P_{available}$, when the antenna is ideally matched on the entire bandwidth, the generated power P_{source}, the actual power generated by the array design, and the power radiated outside the lens P_{lens} by the array design, are **in the order of the mW, when the applied bias voltage is 400V**. Moreover, the table shows the excellent agreement between the detected power estimated by the model and the measured power of the prototype.

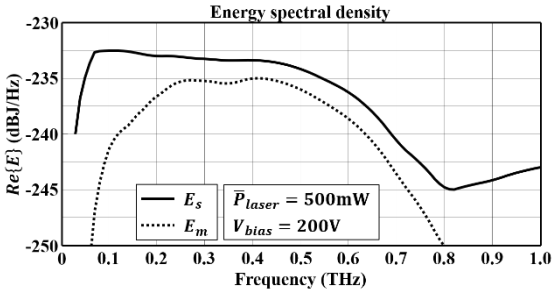

Fig. 6. Simulated energy spectral density of the PCCA. The plot shows the energy spectral densities generated by the arrays E_s (solid lines), and the detected energy spectral densities E_m (dotted line).

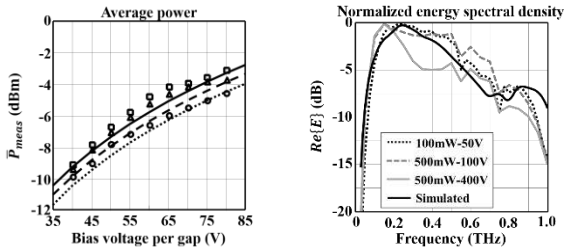

(a) (b)

Fig. 7. Measurements versus model. a) Measured average power as a function of the applied bias voltage; b) measured spectrum for different laser excitation and applied bias voltage.

The normalized amplitude spectra of the measured pulses radiated by the PCCA prototypes under test, for different laser power excitation and bias voltages, are shown in Fig. 7(b), where they are also compared against the normalized real part of the energy spectral density radiated by the reflectors system. The measurements were carried out by using an Electro-Optic (EO) technique in an ambient condition without a controlled atmosphere. The qualitative comparison shows an excellent agreement between the measurements and the estimation of the model for low laser power excitation and bias voltages, thus validating the dispersion analysis performed using our proposed EM model of the QO channel.

Table 1. Power Budget of the PCCA under Test

		Estimated Power				**Measured Power**
P_{laser}	V_{bias}	$P_{available}$	P_{source}	P_{lens}	P_{meas}	
500 mW	200 V	1.76 mW	360 µW	180 µW	130 µW	121 µW
	300 V	3.96 mW	810 mW	410 µW	290 µW	334 µW
	400 V	7.04 mW	1.44 mW	730 µW	520 µW	475 µW

IV. CONCLUSION

In this work, a novel architecture for pulsed photoconductive antennas, which allows high power radiated over a large bandwidth was presented. The solution realized a connected array of photoconductive sources, by implementing an "ad hoc" bias voltage structure, and an optical system to excite the devices. A prototype has been designed and fabricated to maximize the power radiated on a selected bandwidth smaller than the one where the photoconductor source generates energy (bandwidth at -5dB from 0.1THz to 0.6THz). The prototype has been characterized by power and spectrum measurements, validating the effectiveness of the proposed solution for the enhancement of the radiated power for PCAs. The maximum THz average power generated reaches **the order of mW**. The demonstrated power levels are obtained only optimizing the antenna architectures and the relevant modelling.

REFERENCES

[1] P. Jepsen, D. Cooke, and M. Koch, "Terahertz spectroscopy and imaging–modern techniques and applications," Laser & Photonics Reviews, vol. 5, no. 1, pp. 124–166, Jan. 2011.

[2] D. Saeedkia, Ed., Handbook of Terahertz Technology for Imaging, Sensing and Communications, ser. Woodhead Publishing Series in Electronic and Optical Materials. Elsevier Science, 2013.

[3] N. Llombart and A. Neto, "THz time-domain sensing: The antenna dispersion problem and a possible solution," IEEE Transactions on Terahertz Science and Technology, vol. 2, no. 4, pp. 416–423, Jul. 2012.

[4] J. T. Darrow, X. C. Zhang, D. H. Auston, and J. D. Morse, "Saturation properties of large-aperture photoconducting antennas," IEEE Journal of Quantum Electronics, vol. 28, no. 6, pp. 1607–1616, Jun. 1992.

[5] A. Dreyhaupt, S. Winnerl, T. Dekorsy, and M. Helm, "High-intensity terahertz radiation from a microstructured large-area photoconductor," Applied Physics Letters, vol. 86, no. 12, p. 121114, Mar. 2005.

[6] N. T. Yardimci, S. H. Yang, C. W. Berry, and M. Jarrahi, "High power terahertz generation using large-area plasmonic photoconductive emitters," IEEE Transactions on Terahertz Science and Technology, vol. 5, no. 2, pp. 223–229, Mar. 2015.

[7] A. Neto, A. Garufo, G. Carluccio, and N. Llombart, "Photoconductive antenna array," Feb. 9 2017, WO Patent App. PCT/NL2016/050,567. [Online].

[8] A. Garufo, G. Carluccio, N. Llombart, and A. Neto, "Norton equivalent circuit for pulsed photoconductive antennas – Part I: Theoretical model," IEEE Transactions on Antennas and Propagation, vol. 66, no. 4, pp. 1635–1645, Apr. 2018.

[9] A. Garufo, G. Carluccio, J. R. Freeman, D. R. Bacon, N. Llombart, E. H. Linfield, A. G. Davies, and A. Neto, "Norton equivalent circuit for pulsed photoconductive antennas – Part II: Experimental validation," IEEE Transactions on Antennas and Propagation, vol. 66, no. 4, pp.1646–1659, Apr. 2018.